

**Review**

# Upgrading carbonaceous materials: Coal, tar, pitch, and beyond

Xining Zang,<sup>1,2,3,\*</sup> Yuan Dong,<sup>4,5</sup> Cuiying Jian,<sup>6</sup> Nicola Ferralis,<sup>7</sup> and Jeffrey C. Grossman<sup>7</sup>

**SUMMARY**

**Heavy carbonaceous materials (HCMs) such as coal are mostly used for nonrenewable power generation, while derivatives such as tar and pitch are often discarded by-products. Upgrading HCMs for a broad array of potential applications including their use in batteries, membranes, and catalysts could play an important role in the global demand for carbon neutralization. The diversity of HCMs is a technological asset that allows for the direct synthesis of highly customizable materials suited for specific applications. Herein, we will discuss state-of-the-art engineering techniques that can be employed to upscale HCMs and how the nature of the carbon source affects the final product. Further, we illustrate how machine learning (ML) methods can empower the screening of carbonaceous sources from this large family of materials with extremely diverse chemistry. We will also discuss data-driven methods to identify and prioritize the effects of individual processing parameters that could lead to a consistent as well as flexible manufacturing process.**

**INTRODUCTION**

The policy-driven and strategic reduction in the use of fossil fuels for electric power generation has renewed interest in the potential for coal and other heavy hydrocarbons to be used as feedstocks for carbon-based products.<sup>1–3</sup> Such use is not new and in fact dates back nearly a century,<sup>4</sup> but recent advances in developing and scaling up novel nanoscale chemistries with tailored properties and functionalities have opened up new avenues toward the use of coal for noncombustive applications.<sup>5–7</sup> The abundance and ultra-low cost (~\$50 USD/metric ton on average)<sup>8</sup> of coal make it an economically appealing, carbon-rich feedstock,<sup>8</sup> with broad industry opportunities. Figure 1 illustrates examples of coal-derived materials including active carbon for water and air treatment<sup>9</sup> and carbon black for tires.<sup>10</sup> Rare earth metal materials refined from coal and carbon fibers made from coal tar pitch have high additive values that may ultimately make them attractive for commercialization.<sup>11,12</sup> Another strategy to upgrade coals is to leverage their widely tunable chemistry in electronics or other functional structures.<sup>6,13,14</sup> Coal-derived sensors and energy harvesters could be produced at large scale and ultra-low cost, making them appealing for integration with large-volume applications such as construction and infrastructure.

Through millions of years of evolution in varied geological environments, heavy hydrocarbons such as coal provide complex built-in chemical and morphological diversity.<sup>17</sup> Roughly, coal can be divided into four groups: anthracite, bituminous, sub-bituminous, and lignite, listed in order of decreasing rank or maturity levels, aromatic carbon content, and increasing amount of water and aliphatics.<sup>18,19</sup> Aliphatic and aromatic fragments in coal act as functional organic bases, whose different

**Progress and potential**

The global net-zero carbon mission is demanding the reform and revolution of traditional carbon-intensive industries. The policy-driven and strategic reduction in the use of fossil fuels for electric power generation is renewing the interest in the potential for coal and other heavy hydrocarbons to be used as feedstocks for carbon-based products. This perspective highlights the role that complexity and tunability of HCMs (coal, tar, pitch, etc.) play in their thermal upgrading processes. In addition to processing temperatures and ramping/cooling rates, the native chemistries of HCMs play a crucial role in the carbon product crystallinities, morphologies, and conductivities, among other properties. Laser annealing and molecular dynamics simulations can be used to provide general guidelines to select the candidate of HCMs for target properties, and in the future, we expect ML methods to be a valuable direction, together with continuous manufacturing for high-throughput HCM screening, toward a consistent and flexible manufacturing process.



concentration, distribution, and bonding within a stochastic network structure gives form to the different ranks of coal. Besides coal, we also highlight tar and pitch in the discussion, which alongside coal covers a wide range of H:C ratios and aromatic contents in heavy carbonaceous materials (HCMs). Pitch and tar, either extracted from coals or processed from petroleum, provide additional flexibility in their processing compared to raw coals.

The trade-offs and correlations between material complexity and manufacturing complexity have been discussed in the context of solar photovoltaics (i.e., ref<sup>19,20</sup>), where the main idea is that material simplicity (number of heteroatoms, binding configuration, etc.) generally requires complex fabrication processes to achieve the flexible tunability needed in the final application (e.g., controlling doping levels in semiconductors), while complex materials require potentially simpler fabrication steps to achieve the same scope of functionality and tunability.<sup>20</sup> Within this framework, HCMs, as inherently complex materials with a broad distribution of aromatic and alkane fragment sizes and types, hold remarkable potential for achieving different electrical, thermal, and structural properties using simple and versatile processing techniques.

The recent works on upgrading HCMs through thermal engineering (slow or fast pyrolysis, arch discharge, or laser-induced annealing) do not fully leverage and may even downplay (viewing heterogeneity as a negative factor) the role played by the actual carbon source itself in the properties of the final product.<sup>21</sup> In this perspective, we will highlight opportunities for the heterogeneity of HCMs to be considered as an advantage, allowing the direct synthesis of feedstocks to produce highly customizable, advanced materials suited for specific applications. We will also discuss potential precursor screening principles from carbonaceous database for targeted properties and applications and the scaling up to large-scale manufacturing.

## ACHIEVING EXTREME TUNABILITY IN HCMs

### HCM-based opto-electronic and electronic materials

In recent years (Figure 1B), coal has been used as a high-quality carbon-rich precursor to derive nanomaterials including graphene quantum dots (GQDs),<sup>16,22,23</sup> graphene oxide,<sup>6,24,25</sup> nanodiamond,<sup>26</sup> carbon nanotubes (CNTs),<sup>27,28</sup> and more. Products derived from coals are qualitatively related to the built-in chemistry of the coals<sup>29</sup> and the Tour Group has pioneered this area of research for over a decade;<sup>5,16,22</sup> an example of their work is shown in Figure 1B by the work of Ye et al., which demonstrates that various size GQDs can be oxidized from anthracite and separated by crossflow filtration.<sup>16</sup> The emission wavelength of such GQDs depends on their sizes, which can also be controlled by the synthesis temperature.<sup>16</sup> Nilewski et al. used poly(ethylene glycol) (PEG) to functionalize the stabilized GQDs as an efficient antioxidant.<sup>15</sup> On the other hand, the complex aromatic network of coal can be a versatile resource to extract GQDs with controllable aspect ratios in different supercritical fluids.<sup>23</sup> The derived nanocarbon materials have been used as a new platform for opto-electronics<sup>30</sup> and biomedical imaging.<sup>23</sup>

The above examples of coal-derived nanomaterials have been processed primarily by thermal annealing and chemical reduction, and their differences mainly arise from aromatic content and the smallest aromatic sizes of the functional unit that can represent the properties of the coal when tailored.<sup>31</sup> Anthracite coals and bituminous coals can serve as a precursor for high-yield graphitic carbon material synthesis including CNTs,<sup>32</sup> fullerenes,<sup>33</sup> and large-size (>100 nm) graphene sheets,<sup>34</sup>

<sup>1</sup>Department of Mechanical Engineering, Tsinghua University, Beijing 100084, China

<sup>2</sup>Key Laboratory for Advanced Materials Processing Technology, Ministry of Education, Beijing, Tsinghua University, Beijing 100084, China

<sup>3</sup>State Key Laboratory of Tribology, Tsinghua University, Beijing 100084, China

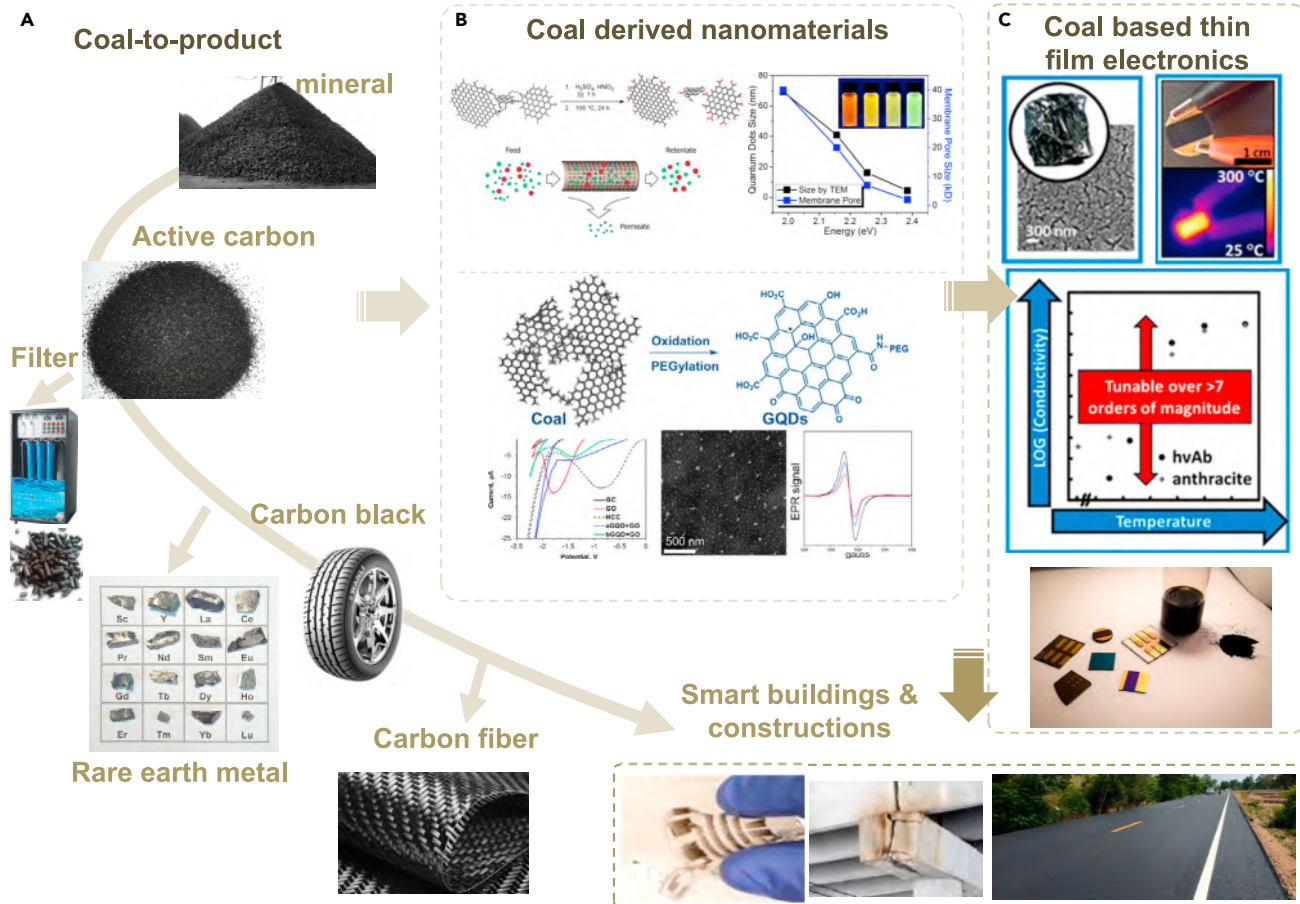
<sup>4</sup>School of Mechanical Engineering, Hangzhou Dianzi University, Hangzhou 310018, China

<sup>5</sup>Shenzhen Artificial Intelligence Industry Association, Futian, Shenzhen 518031, China

<sup>6</sup>Department of Mechanical Engineering, York University, 4700 Keele Street, Toronto, ON M3J 1P3, Canada

<sup>7</sup>Department of Materials Science and Engineering, Massachusetts Institute of Technology, Cambridge, MA 02139, USA

\*Correspondence: [xzang@tsinghua.edu.cn](mailto:xzang@tsinghua.edu.cn)  
<https://doi.org/10.1016/j.matt.2021.11.022>

**Figure 1. Noncombustive uses of coal**

(A) Nonconventional coal-to-product routes.

(B) Coal-derived nanomaterials, including GQDs,<sup>15,16</sup> graphene nanoribbons, and nano diamonds. Copyright © 2015 and © 2019, American Chemical Society.

(C) Coal-based thin-film electronics including photovoltaics and potential application in smart building and constructions with sensing electronics. Copyright © 2016, American Chemical Society.

due to the large aromatics. Lignite coals, which contain comparably much smaller aromatic constituents, have mainly been used to derive carbon quantum dot diameters in the few-nanometer size range.<sup>35</sup>

Coal-based thin-film electronics represent another potential direction for scalable upgrading of coals.<sup>13</sup> Keller et al. first presented a coal-based conductive thin-film processing route (Figure 1C), which includes a nanoscale powder supernatant floatation to select dispersive coal powders, a thin-film spinning process to make a uniform coating, and a thermal annealing step to increase the film conductivity at different temperatures.<sup>13</sup> The temperature-driven dehydrogenation reactions determine the H:C ratio,  $sp^2$  content, localization length, and disorder of the annealed coal thin films, which behave differently for different coal feedstocks. Both the electrical conductivity and optical band were shown to be highly tunable for different types of coal with simple annealing. The resulting electron-hole conductivities follow a variable range hopping process in a three-dimensional disordered structure as:

$$\sigma \propto e^{-(T_0/T)^{1/4}}$$

where  $k_B T_0$  is the characteristic hopping energy or the average energy spacing near the Fermi level.<sup>36</sup> The difference in fitted  $T_0^{1/4}$  for anthracite and bituminous coals reflect the diversity of structures and properties between coals. As an example application, an anthracite coal thin film annealed at 950°C, with the largest sp<sup>2</sup> clusters and high conductivity of 10<sup>3</sup> S/cm, was shown to be a robust joule heater that can operate stably in air at 285°C, which could be of interest in applications ranging from biomedical thermal therapy<sup>37</sup> to defogging and defrosting.<sup>38,39</sup> Besides joule heaters, coal-based thin films may hold promise in passive electronic components including resistors, capacitors, sensors, and inductors.<sup>40,41</sup> Since the precise control of mean free path and carrier mobility is still difficult, we do not imagine that coal-based electronics will replace silicon-based electronics, although the mobility and conductivity can be controlled by tuning the conjugated aromatic structures, which may provide opportunities for using coal-based materials with semiconducting behavior in active electronic components, including metal-oxide-semiconductor field-effect transistors (MOSFET), amplifiers, and logic gates<sup>42,43</sup>

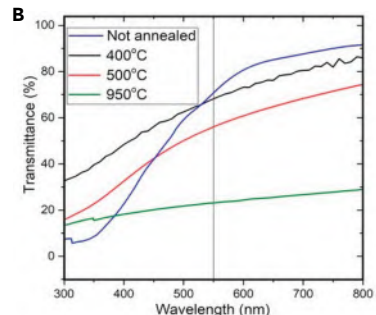
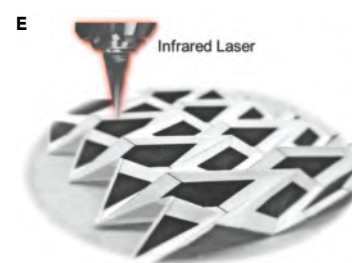
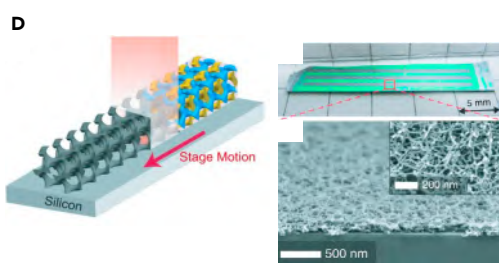
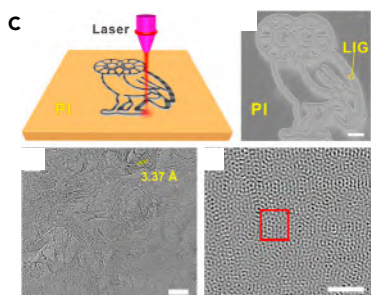
#### Laser engineering of HCMs and direct print devices

In contrast to grainy coal powders, tar and pitch are two materials from the HCM family that behave like a sticky liquid and semi-solid, which can be processed in solution more easily. Using tar as an example, tar thin films processed with an organic solvent such as dichloromethane (DCM) and N-methyl pyrrolidone (NMP) can provide a more homogeneous control of the chemistry and morphology as shown in Figure 2A. Petroleum tar, a by-product of ethylene cracking, has few useful applications other than burning into black carbon. Morris et al. annealed spin-coated tar thin films at up to 950°C to tune their transparency and conductivity to make transparent heaters (Figures 2A and 2B).<sup>38</sup>

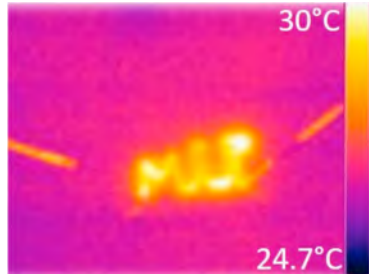
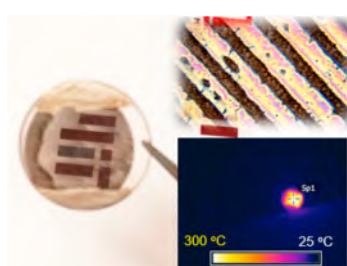
By controlling the annealing temperature (Figure 2B), tar thin films can achieve a wide range of transparencies (23%–93%) and corresponding sheet resistances (2.5 ohm/sq to 1.2 kohm/sq). The tar films annealed over 950°C are metallic, with transparency-conductivity relationships similar to that of reduced graphene oxide (rGO) transparent thin films and graphene thin films.<sup>38</sup> As such, the carbon-based thin films with similar transparencies present similar heating temperature plateaus, although tar-based transparent heaters can reach 285°C, while rGO and graphene-based thin films generally work below 200°C.<sup>38</sup>

The temperature limitations of furnace annealing and the relatively slow heating process leads to a large loss in total mass. In the case of tar, uniform spin-coated thin films with initial thicknesses of several microns drastically shrink to a few tens of nanometers, with over 80% mass loss. Compared with furnace annealing, laser ablation or laser annealing can reach much higher local temperatures (thousands of degrees Kelvin),<sup>47</sup> with faster temperature ramping<sup>48</sup> and also enhanced spatial control and resolution.<sup>49,50</sup>

Laser annealing has been applied on polymeric substrates to produce carbon materials with controllable properties such as porosity, crystallinity, and conductivity (Figures 2C–2E). Lin et al. demonstrated laser-induced graphene (LIG) on commercial polyimide in 2014 (Figure 2C); thereafter, many works have employed laser annealing as a simple and facile method to pattern graphene on polymeric materials including polymer films, cloth, wood, and even bread.<sup>44,51</sup> As shown in Figure 2D, laser-annealed self-assembled copolymer thin films can have tunable hierarchical three-dimensional porosity by tuning the block co-polymer mixtures and lasing

**A Furnace annealing of tar thin film****Laser ablation: better temperature and spatial control****F Laser printed tar based devices**

Local heating: suitable for different substrates and compatible with lithography processes.

**G****H**

**Figure 2. Laser engineering of polymer materials and HCMs**

- (A) Schematic to process tar thin films and the optical images of as-deposited and furnace-annealed tar thin films.
- (B) Optical transparency plots of tar thin films annealed at different temperatures, reflecting a decrease in optical bandgap upon heating temperatures.<sup>39</sup> Copyright 2019, Wiley.
- (C–E) Laser-induced functional carbon materials.
- (C) Laser-induced porous graphene on polyimide.<sup>44</sup> Copyright © 2018, American Chemical Society.
- (D) Laser scribed hierarchical porous carbon on co-polymer.<sup>45</sup> Copyright © 2019, under the use term of ACS Editors' Choice.
- (E) Laser-printed molybdenum carbide-graphene on paper.<sup>46</sup> Copyright © 2018, Wiley.
- (F) Schematic of tar thin-film processing and patterning conductive feature via laser annealing.
- (G) An infrared camera image of laser-printed conductive feature heated up.
- (H) Heating responses under 60 V bias of tar heaters.<sup>14</sup> Copyright © 2020, AAAS.

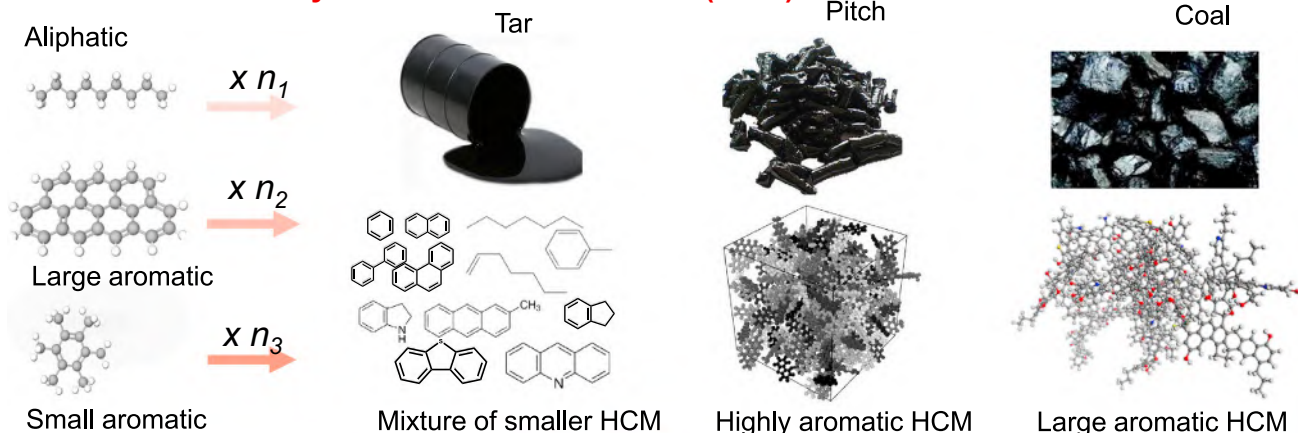
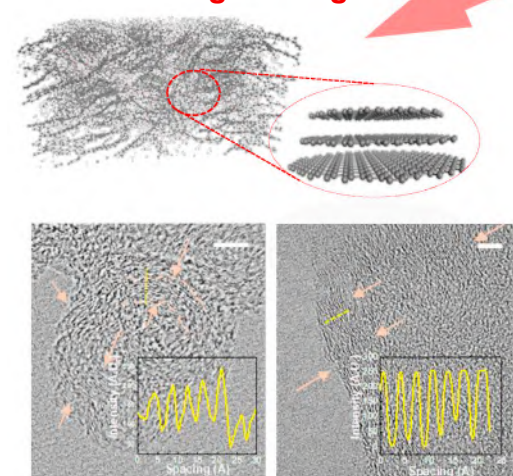
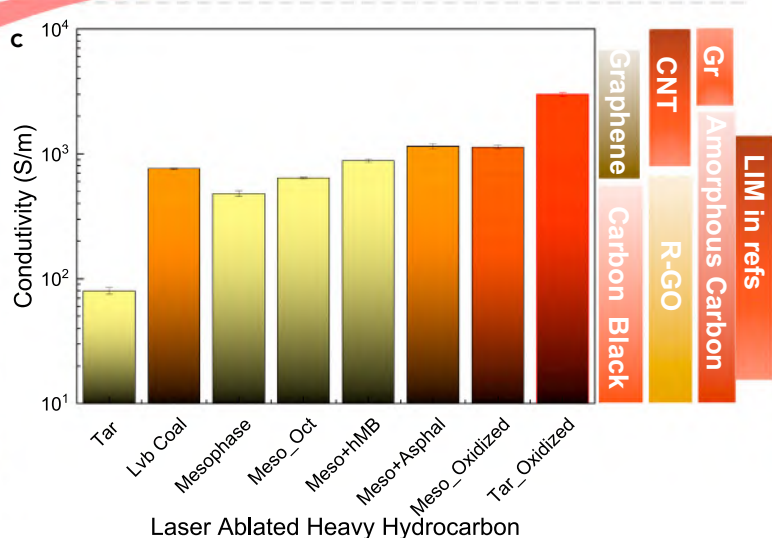
parameters.<sup>45,52</sup> Molybdenum carbide-graphene composite electrodes can be laser-printed on a range of paper substrates (A4 paper, tissue, wiping paper, etc.) in ambient environments, giving foldable paper multiple functions including sensing and energy storage.<sup>46</sup> Zang et al. showed a laser annealing process to carbonize tar thin films and printed a joule heater (Figures 2F–2H).<sup>14,39</sup> The H:C ratio and  $sp^2$  aromatic content of films at various levels of annealing can be obtained from Urbach tail energies derived from the films' visible absorption spectra.<sup>53</sup> From this analysis, it was shown that the H:C ratio in tar thin films decreases from ~1.20 to ~0.95 upon

laser annealing, compared with the same films processed by furnace annealing, which decrease in H:C ratio to ~1.05. Correspondingly, the aromatic content in tar thin films increases from ~0.35 to ~0.55 after laser annealing, and to ~0.47 by furnace annealing. With laser annealing, the rapid heating rate to graphitization temperatures leads to almost immediate transformation with lower material loss (~50%) compared with furnace annealing (>80%). The laser printing process can also be customized to fabricate thin-film electronics, in which the nonablated tar is removed by solvent stripping, as shown in Figures 2F and 2G. The transparency of the annealed film can be tuned by the lasing line spacing to maximize the visibility while maintaining conductivity above the threshold needed for a transparent heater. From raw material to devices, tar-based transparent heaters require two steps (a coating and an annealing process), which is favorable in terms of process complexity compared with the use of rGO and graphene to make transparent thin films.<sup>54</sup>

Furthermore, the unique chemical diversity of HCMs can be considered a technological asset that allows for producing highly customizable, advanced materials suited for specific applications by laser-induced reactions. The customizability of HCMs originates from their molecular constituents as well as processing parameters. Instead of lasing individual HCMs, they can be investigated as a collection of organic fragments, as shown in Figure 3A. Tar is usually rich in hydrogen and has low aromatic content. Pitch, on the other hand, typically has high aromatic content with low H:C ratios. For coal, the H:C ratio is intermediate, as is its aromatic content. Coals have higher density and molecular weight, and their unit structure has a more complex and diverse hydrocarbon structure compared with tar and pitch (Figure 3A). The laser-ablated products show a strong dependence on the precursor properties, i.e., the original  $sp^2$  and  $sp^3$  ratio and aromatic content. For example, ablated tar shows para-crystalline nanoscale (~5 nm) graphitic sheets mediated with amorphous organics in between the layers, while laser-ablated coal shows few layers of graphitic stacks from high-resolution transmission electron microscopy images (HRTEM) as shown in Figure 3B. Furthermore, the original highly aromatic ( $sp^2 \sim 1.0$ ) mesophase shows a disturbed amorphous structure after annealing. The experimental results indicate that aliphatic chains and the initial aromatic cores both play an essential role in the resulting stacked graphitic structures.

Raman signatures are commonly used to characterize the structures of carbon materials by measuring the D peak near  $1,350\text{ cm}^{-1}$ , G peak near  $1,600\text{ cm}^{-1}$ , and 2D peak near  $2,750\text{ cm}^{-1}$ . The 2D peak reflects graphitic stacking, while the D/G peak ratio ( $I_D/I_G$ ), G peak position, and full width at half maximum (FWHM) need to be cross-compared to evaluate the localization length (i.e.,  $L_a$ ) and  $sp^2$  content of the carbon product.<sup>55–57</sup> More details of the Raman analysis of carbon with different structures can be found in papers by Ferrari et al.,<sup>55,56</sup> Matthews et al.,<sup>58</sup> and Pimenta et al.<sup>59</sup> Small aromatic additives can promote the crystallinity of laser-ablated HCM mixtures, resulting in a high  $I_{2D}$  peak and large fitted in-plane crystallite size  $L_a$ .<sup>59,60</sup> By tuning the crystalline structures of their internal hydrocarbon network structures, broadly distributed conductivities of ablated HCM thin films were obtained.<sup>14</sup> The higher graphitization of ablated low-volatile bituminous (LvB) coal leads to an order of magnitude higher conductivity (~800 S/m) compared with ablated tar (~80 S/m), while the poorly graphitized ablated mesophase pitch (MP) still shows a large conductivity (~500 S/m) due to its interconnected structure (Figure 3C).

For comparison, the longitude electrical conductivity of pure metallic CNT can be as high as  $10^6$  to  $10^7$  S/m and defect-free graphene  $10^8$  S/m.<sup>61</sup> Monolayer graphene produced by chemical vapor deposition and mechanical exfoliation exhibit high

**A Toolbox of heavy carbonaceous materials (HCM)****B Laser engineering****C****Figure 3. Laser-induced chemical evolutions of HCMs**

(A) Compositions of three typical heavy carbonaceous materials (tar, pitch, and coal) that are mixtures of aliphatics and aromatics with different sizes and ratios.

(B) Laser-ablated stochastic graphitic system from HCMs and their crystalline structures resolved by transmission electron microscopy (TEM).

(C) The conductivities of laser-ablated HCMs thin films and their hybrid thin films compared with the conductivities of synthetic carbon materials. Copyright ©2020, AAAS. LIM: laser-induced materials.

in-plane conductivities up to  $10^4$ – $10^5$  S/cm, while thin film multiwall CNTs' (MWCNTs) forests have a conductivity range of  $10^3$ – $10^4$  S/cm (Figure 3C; Table 1).<sup>61,62</sup> Thin films made of porous graphene, CNT forests, and CNT yarns possess much lower conductivity in highly defected percolated networks (Table 1). LIG from polyimide shows  $10^1$ – $10^3$  S/cm conductivity,<sup>48</sup> which is two orders of magnitude less conductive compared with porous microcrystalline graphite. The percolation structure and connectivity are crucial for film conductivity, where the presence of molecular bridges can greatly increase the charge transfer and electron coupling.<sup>63,64</sup> In turn, they can enable conductivities similar in magnitude to graphite-like networks. Such phenomena have been discussed in refs.,<sup>30,31</sup> where it was shown that when controlling the initial HCM selection and additive agents such as hexamethylbenzene (hMB) and octane, the conductivities of HCM thin films can be increased from below 100 to  $\sim$ 1,000 S/m (Figure 3C). The co-existence of

**Table 1. Conductivities of laser-induced carbon materials**

Material type	Raw material	Method	Conductivity (S/cm)	Ref.
CNT forest	N/A	Chemical vapor deposition	10 <sup>2</sup> –10 <sup>4</sup>	Jiang et al. <sup>66</sup>
LIG	Polyimide	Laser annealing	25–10 <sup>3</sup>	Lin et al. <sup>48</sup> and Chyan et al. <sup>51</sup>
Furnace-annealed coal	Coal	Furnace annealing	10 <sup>3</sup>	Keller et al. <sup>13</sup>
Furnace-annealed tar	Petroleum tar	Furnace annealing	10 <sup>2</sup> –10 <sup>3</sup>	Morris et al. <sup>39</sup>
Laser-ablated HCMs	HCMs	Laser annealing	10 <sup>2</sup> ~3 × 10 <sup>3</sup>	Zang et al. <sup>14</sup>

LIG: laser-induced graphene.

small aromatics (such as hMB) and aliphatics (such as octane) bridges the original aromatic networks, which can in turn promote the graphitization of HCM thin films during annealing. Furthermore, it was shown that low-temperature oxidation of MP thin films and tar thin films (300°C, in air, 4 h) provides over 2.4 times and over 36 times higher electrical conductivity after laser annealing compared with nonoxidized films. Laser-ablated oxidized tar with large graphitic domains shows a higher conductivity (~2,990 S/m) than laser-ablated oxidized MP (~1,133 S/cm). This difference can be attributed to the oxygen-induced crosslinking of aromatic clusters obtained through low-temperature annealing, which turns into structures with a substantially higher degree of conjugation and stacking between aromatic sheets.<sup>65</sup> The understanding of the functionality of each component of HCMs provides guidelines to tune the morphology and conductivity of as-annealed products by optimizing the composition of the heterogeneous mixtures of HCM feedstocks and laser processing parameters.

## UNDERSTANDING THE TUNABILITY OF HCMs WITH COMPUTATION

### Molecular dynamics simulations of the high-temperature reactions of HCMs

To achieve full control over the tunability of HCMs, it is crucial to capture reaction pathways induced by high-temperature laser annealing. The reaction pathways can not only guide the choices of annealing parameters to ensure the consistency of batch production, but also form the foundation to develop reaction networks that bridge the initial molecular constituents with the properties of ablated samples. In this context, atomistic-scale modeling provides a powerful tool to reveal such reaction details. Density functional theory (DFT), kinetic Monte Carlo, and classical molecular dynamics based on reactive forcefields (ReaxFF), to name a few, have all been used to investigate reaction pathways of organic materials.<sup>67–70</sup> While the focus of such works was outside the scope of upgrading HCMs, they shed light on how HCM reactions could be handled (especially the applicability of ReaxFF as reviewed later in this section). Compared with chemicals with well-defined molecular representations, the intrinsic complexity of HCMs imposes additional, significant challenges on atomistic modeling of their reactivities during thermal processing, due to the lack of microscopic structural models.<sup>71,72</sup>

To take the broad spectrum of compositions, crystallinity, and molecular geometries into account, several strategies have been proposed in the literature to build proxies for HCM samples. For instance, Mathews and co-workers developed a variety of image-analysis packages and construction tools to create atomistic models that capture the structural diversity and partial ordering of coal and char samples.<sup>73–75</sup> The so-constructed models have been used to investigate combustion and pyrolysis of coal and char.<sup>71,75</sup> Li et al.<sup>31</sup> employed an in-house-developed protocol to generate atomistic representations to match target H/C, O/C ratios of sub-bituminous coal samples. This protocol employs a series of short molecular dynamics runs to relax

representations consisting of pseudo molecular fragments and bridges. Such an approach demonstrates promising potential for the prediction of electronic properties of untapped, i.e., unprocessed, HCMs. To correlate aromatization of kerogens and their visible electronic absorption edge, Ferralis et al.<sup>53</sup> built their molecular representations by mixing H/C/O atoms or hydrocarbon molecules to match specific H/C and C/O ratios. For all these approaches, the computational molecular systems contain a mixture of proxy molecular compounds that can reproduce structural and spectroscopic characteristics with experimental measurements. In addition, although the majority of the aforementioned strategies were intended for applications other than probing reaction pathways, they clearly demonstrated the complexity of HCM models that should be considered to fully leverage the potential insights from computational studies. Jian et al.<sup>14,76,77</sup> showed two approaches based on characteristics of a specific HCM type to explore and compare reaction pathways. Molecular representations for tar were built by mixing commercially available compounds to specifically match densities, H:C ratios, and aromatic contents with experimental counterparts.<sup>14,77</sup> On the other hand, for coal and pitch, a single type of polycyclic aromatic compound was adopted as a representative of “averaged” structures, by the molecular representations of MP used for carbon fiber synthesis.<sup>14,76,78</sup> The rationale behind these two approaches is to probe the effect of key differences (aromatic contents and H:C ratios) on reaction pathways by removing possibly insignificant details. Figures 4A–4C summarize the models used in refs.<sup>14,76,78</sup>

The second challenge in applying atomistic modeling to gain insight into reaction pathways in these materials arises from the size and timescale differences between what can be measured experimentally and what can be modeled computationally. Such a challenge is of course well known and encountered in simulating the kinetics of heavy oil molecules, biomolecules, and inorganic substances,<sup>79–81</sup> among many other materials. To observe desired conversions (e.g., carbonization, graphitization, etc.), energy inputs into the system have to exceed certain thresholds,<sup>82–84</sup> thus requiring sufficient thermal energy to enable the corresponding reactions and re-orderings within the timescale attainable in the simulation. A standard practice in the literature is to adopt the Arrhenius equation to scale up reaction temperatures in simulations:  $k = Ae^{-E_a/RT}$ ,<sup>85,86</sup> where  $k$  is the rate constant (units depending on specific reactions),  $T$  is the absolute temperature (K),  $E_a$  is the activation energy (in the same units as RT), and  $A$  is the pre-exponential factor (in the same units as  $k$ ). The elevated temperatures allow for fast conversions and thus achieve materials conversions within  $\sim$ ns, which can be captured during the simulations, compared with  $\sim$ μs in the laser annealing experiments or  $\sim$  s during furnace annealing. This scaling intrinsically represents an approximation, and the heterogeneity of HCMs brings additional uncertainties to a one-on-one mapping of processing conditions (for instance, the determination of  $E_a$  is mostly based on trial and error). It is important to note that estimations factored into the temperature scaling may not be of significant concern for the purpose of capturing fast dynamics other than tracking long-time growth.<sup>87,88</sup>

With the help of kinetics scaling, the complexity of HCMs still restricts the methods that can be adopted. For example, *ab initio* molecular dynamics has been rarely used for probing reaction pathways of HCMs and further developing reaction networks, given its high computation demands compared with the use of classical force fields.<sup>89</sup> In this context, the development of ReaxFF offers an appealing compromise with the possibility of higher accuracy, although with the trade-off of greater computational costs compared with most other classical force fields.<sup>70</sup> Extensive works in the literature have employed ReaxFF to investigate initial reaction mechanisms

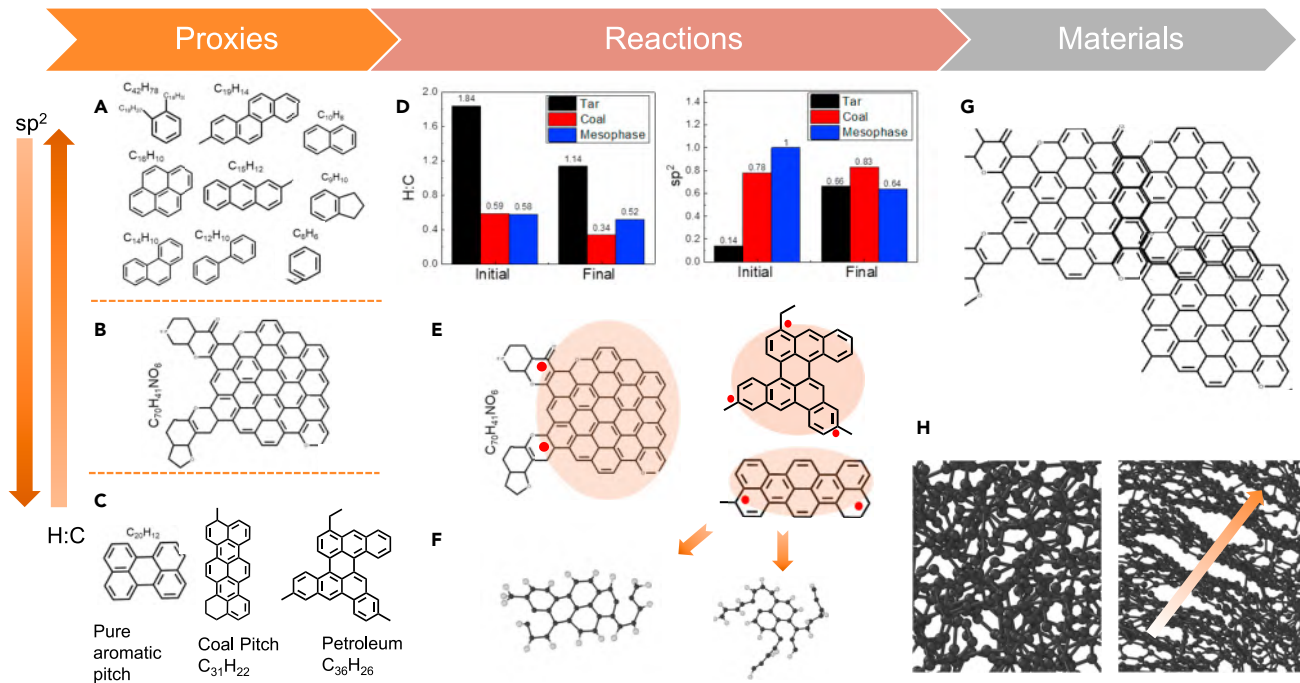


**Figure 4. Thermal treatment and laser-ablation-induced chemical reaction of HCM**

(A–C) Proxy models adopted for tar, coal, and pitch.

(D) ReaxFF results of H:C ratios and  $sp^2$  contents.

(E) Active sites of representative HCMs.

(F) Radicals formed at relatively low (left) and high (right) temperatures.

(G) Ring condensations observed in coal.

(H) ReaxFF snapshots of amorphous (left) and (graphite) materials.<sup>77</sup> Copyright © 2019, Elsevier Ltd.

and kinetics associated with combustion and pyrolysis of lignite, coal, and alkane fuels<sup>86,90,91</sup> as well as the formation of soot.<sup>92</sup> The reaction pathways of HCMs under high temperatures have been explored recently using ReaxFF<sup>14,76,77</sup> to study the effects of structural characteristics and processing conditions, the growth of solids from HCMs, and the development of general guidelines to exploit the tunability of HCMs for different applications.

An example of the use of ReaxFF-based molecular dynamics to explore how H:C ratios, aromatic contents, and processing conditions in HCMs modulate the reactivities and final products is shown in Figure 4D, where it was found that  $sp^2$  content of tar after laser ablation, while increased, is still lower than that of coal. Excessive presence of hydrogen can inhibit ring condensation from small aromatic molecules,<sup>77</sup> which has the implication that decreasing the H:C ratio can help with the formation of aromatic sheets (Figures 4D and 4G). Laser-induced graphitization reactions often require an increase in the  $sp^2$  content, which has been performed by multiple lasing strategies and defocusing strategies. In the work by Chyan et al.<sup>51</sup> and Beckham et al.,<sup>84</sup> polymer substrates including complicated natural carbonaceous coconut shells and photoresists are converted to amorphous carbon with reduced H:C ratios and promoted  $sp^2$  contents, which are then converted into graphene.

However, if aliphatic contents are too low, a high temperature will result in ring-opening and thus is deleterious for ring condensation, as was observed for pitch

models with 100% aromatic contents (Figures 4C and 4D).<sup>14,76</sup> These simulations point to the range of potential for customized materials, amorphous networks, or crystalline graphite to be produced by careful selection of feedstocks. Further tunability can be introduced by the inclusion of  $sp^3$  carbons, where the sites of these  $sp^3$  carbons play important roles in determining reaction pathways as well as characteristics of the final materials.<sup>76</sup> Pitch molecules with  $sp^3$  carbons on the side chains (petroleum pitch, Figure 4C) can have multiple reaction pathways, which diversify the compositions of heavy radicals and interfere with ring condensations (left, Figure 4H). In contrast, the presence of  $sp^3$  carbon in the core area (coal pitch, Figure 4C) can promote the formation of heavy radicals mainly through cyclic cleavages (Figure 4E). These aryl radicals facilitate ring condensation while preserving the initial molecular arrangement (right, Figure 4H). Regarding processing conditions, for all types of HCMs, at relatively low temperatures (e.g., 2,000 K), aryl radicals are present, while at relatively high temperatures (e.g., 4,000 K), they can significantly disrupt aromatic rings, leading to the formation of acetylic chains (Figure 4F).<sup>76,77</sup>

The above results and analysis from simulations of HCMs illustrate how the complexity of molecular moieties offers a wide range of reactivities and reaction pathways. Several general guidelines can be proposed for selecting raw samples and determining processing conditions. To obtain graphitic structures, raw samples that can provide both carbon sources and backbones are preferred. The presence of  $sp^3$  in the ring areas, while promoting reactivities, might help to limit reaction pathways and thus preserve the initial molecular ordering. Meanwhile, temperatures should be high enough to allow for the swift cleavage of light components and reasonably low to limit the disruption of aromatic rings. The diversity in growth/condensation of aromatic rings induced by feedstock and manufacturing ultimately lead to different properties of processed materials (e.g., porosity, conductivity, transparency, and structural stability). It is also noteworthy that atomistic modeling of amorphous materials has broad application beyond HCMs. For organic matter, the design of fuels is a close example, where molecular mixtures are investigated to determine the contributions of individual components to the combustion phasing and production of emissions.<sup>93,94</sup> For inorganic substances, amorphous silicon and its hydrogenated counterparts have been extensively studied, given their important roles in thin-film transistors, multi-junction solar cells, image-sensor arrays, etc.<sup>95,96</sup>

In addition, probing reaction pathways by atomistic modeling can also help to calibrate reaction rules that are the foundation of molecular-level kinetic models for petroleum refining.<sup>97,98</sup> In these kinetic models, pre-defined pathways are used to generate reaction networks to predict product yields from mixed reactants. Previous works in these broad applications can help address challenges faced by processing HCMs; for instance, the atomistic construction of amorphous silicon and amorphous carbon typically starts with refining pair correlation functions through fitting experimental measurements, suggesting that to model HCMs, such key structural factors are worth searching for.<sup>88</sup> In addition, ML-based potentials/force fields are emerging for simulating amorphous carbon to balance accuracies (comparable with *ab initio* molecular dynamics) and computational costs (similar to force-field-based approaches).<sup>99,100</sup> Nevertheless, as reviewed above, computational studies have been focusing on explaining experimental observations and proposing general guidelines that may not be readily applicable to manufacturing processes. In other words, a full map of HCM conversions is still far from complete, although the current limiting factors also provide future opportunities for further research as discussed below.

First, the importance of compositions on reactivity under high temperatures needs to be assessed systematically. While specific compositions of HCMs vary across a broad spectrum, major elements of all HCMs are H and C, and classifying compositions into different categories would help to pinpoint key structural descriptors determining reaction networks. Second, it is crucial to distinguish between statistically averaged descriptors (e.g., H:C ratio and aromatic content) and individual molecular characteristics (e.g., chemical structures), especially for highly heterogeneous HCMs. The strength of atomistic modeling lies in revealing details at the cost of decreasing time and length scales. The removal of insignificant details can help to scale up and further predict system reactivities. Along with these directions, data analysis tools, such as principal component analysis and diffusion maps, can be employed to rank the relative importance of structural factors.<sup>101</sup>

From a processing point of view, kinetics scaling based on the Arrhenius equation typically speculates experimental temperatures. To address this, one-to-one mapping between simulation conditions and operational parameters of the laser can be established through building temperature profiles using a finite-difference time-domain method in real-time laser manufacturing.<sup>102</sup> Furthermore, with a one-on-one mapping, elevated temperatures may still downplay the role of hierarchical reactions that occur on time scales of ~s. In this regard, it is also clear that advancements in parallel algorithms, software, and hardware will greatly help to increase the computation speed and enable reactive simulations on the order of  $\mu\text{s}$ .<sup>87,88</sup> In addition, the Deep Potential scheme, which has been used to develop force fields for toluene, water, copper, etc., from *ab initio* calculations, can also help to further upscale the efficiency of the existing ReaxFF.<sup>103,104</sup> Lastly, with sufficient fundamentals revealed, similar to molecular-level kinetic modeling employed in petroleum refining,<sup>105</sup> frameworks based on pre-defined reaction roles (pathways) can be established to generate large-scale reaction networks. These networks can then link reactants to final products, for which crystallinities, electronic structures, and carrier mobilities can be evaluated using a variety of computational methods ranging from molecular dynamics to coarse-grained modeling, to DFTs, and to Monte Carlo.<sup>31,76</sup> That is, predictive results can be obtained to quantitatively guide the design of the upgrading/manufacturing process.

### Decoding and screening HCMs

As described above, a major challenge with computational approaches applied to HCMs is to employ models with both high fidelity and efficiency at different scales (nano-micro-macro) and for different physical or chemical reactions during the manufacturing processes.<sup>106,107</sup> Toward this end, ML techniques and genetic algorithms can potentially provide reliable predictive screening of the chemical near-infinite parameter space of HCMs due to both their chemical complexity and range of processing kinetics in different manufacturing methods.<sup>108–110</sup>

One important direction lies in the rational decoding of HCMs into functional structure units, as for example explored by Liu et al.<sup>111</sup> in a combined DFT and genetic algorithm approach, to build a chemical structure relationship with Raman spectra of HCMs. The genetic algorithm was used to search for ratios of candidate molecular components with composite Raman spectra that fit best to the experimental spectra, allowing for characterization of molar H/C ratio, aromatic cluster size, and mole fraction of bridgehead aromatic carbon. This result highlights the potential correlation between constituents of carbonaceous materials with structural, chemical, and physical features (Figures 5A and 5B). A similar idea was recently adopted by Salley et al.,<sup>112</sup> where the spectral signatures of Au nanoparticles were used as an objective function and the ML models trained to find new morphologies to obtain the desired

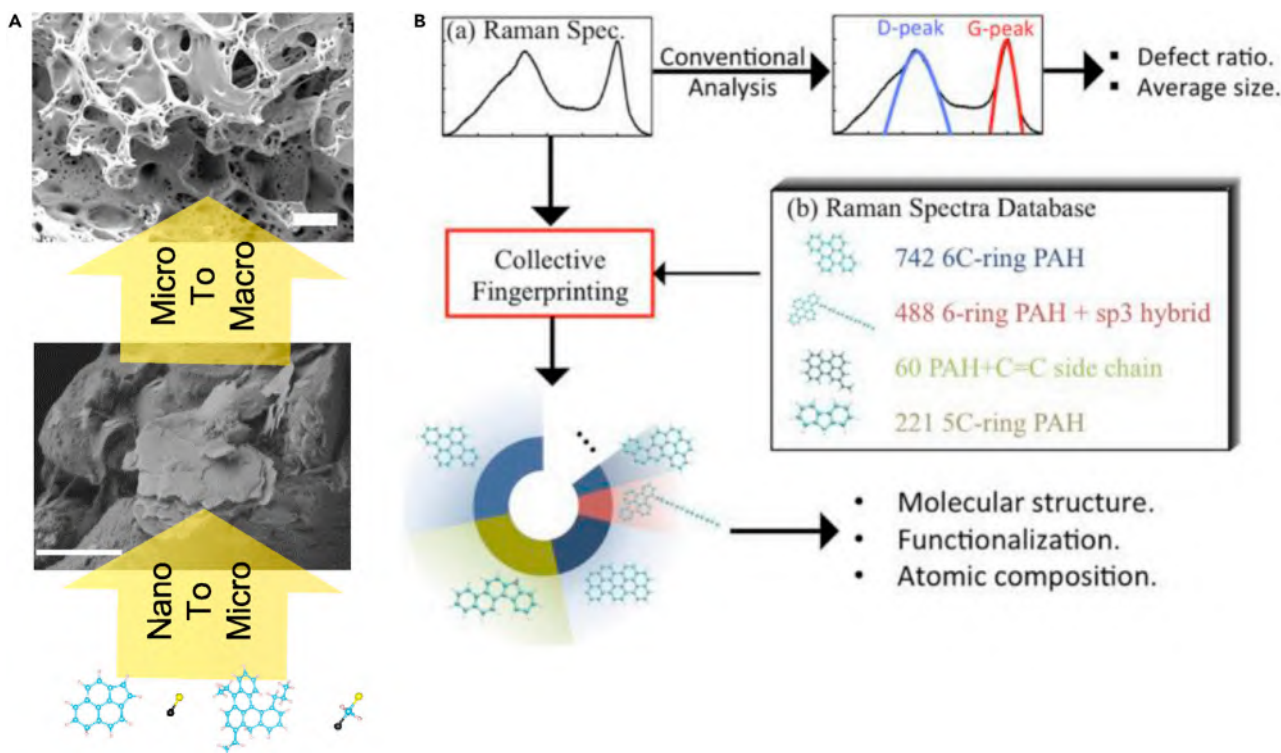


**Figure 5. Decoding HCMs and screening the pool of HCM for target properties**

(A) Schematic of organic units that assemble the nano-micro-macro scale structures of carbonaceous materials.

(B) An example of a genetic-algorithm-based fingerprinting approach to resolve molecular-level information from Raman spectra.<sup>111</sup> Copyright © 2016, Elsevier Ltd. Copyright © 2020, Elsevier Ltd.

spectrum, indicating the potential for spectral as inputs for ML to accelerate materials discovery. Combining laser and *in situ* Raman analysis, laser parameters can also be automatically tuned using ML methods, for example, Bayesian optimization, to identify and prioritize the effects of individual processing parameters, leading to a more consistent and flexible manufacturing process.<sup>113</sup>

ML methods can also accelerate the computation of reactions involving HCMs, for example using deep learning with a parameterized ReaxFF framework.<sup>114,115</sup> The effects of precursor (atom positions) and reaction conditions (nonequilibrium processes) on carbonaceous material properties can be used to train ML models. The current versions of ReaxFF require charge equilibrations to handle the electrostatic interactions, which significantly consumes additional resources during a typical simulation run. Deep learning may help to remove charge equilibrations by factoring the charge into the local environment of each atom.<sup>116</sup> In other words, instead of adjusting charges of all atoms, if needed, a “correction” term can be added to the potential energy by examining the neighborhood of each atom that is already being stored and calculated for other types of pairwise interactions.<sup>117</sup> We expect that the use of multiple ML approaches combined with the expanding dataset of coal upgrading experiments could continuously refine these models to accelerate the optimization of upgrading carbonaceous materials.

## CONTINUOUS MANUFACTURING

In this last section, we discuss the prospects of upscaling the manufacturing of HCM films with desired properties targeting a range of potential applications. Scalability

is quite a common issue in the recent development of advanced manufacturing technologies,<sup>118</sup> such as two-photon polymerization, as the nanoscale/microscale properties can change if just simply scaled up in size.<sup>119</sup> Development of continuous manufacturing strategies will require customization of raw materials, dispersion agents, chemical additives for the deposition, thinning, laser ablation, laser printing, and packaging facilities that can be integrated to an automated production line. Laser-printed conductive features can also be transferred to other stretchable substrates such as Ecoflex as shown in [Figure 6A](#), which can further broaden applicability.

For any form of tar and pitch, a lot of work needs to be done to customize their rheology, dispersion, and feasibility with the manufacturing stream. Solid HCMs such as coal need further study to make suspensions that are compatible in a coating process. As shown in [Figure 6B](#), a fully vertically integrated continuous manufacturing process can transform coal-based feedstocks into solid continuous films for electronics in a roll-to-roll (R2R) manufacturing process. Such films will be tuned through chemical functionalization and laser heating. Doping, in general, is a sensitive and crucial process for determining the band structure and conductivity of materials and can be deployed by lasing with additives that decompose to supply targeted dopants.<sup>121</sup> A next step would be to employ continuous manufacturing of HCM-based films with properties tailored for a given target application. Laser integrated roll-to-roll manufacturing is highly customizable for thin-film electronics, while a few recent works by Luong et al.<sup>5,120</sup> show that flash heating can produce graphene solid products at gram scale. As shown in [Figure 6C](#), a flash joule heating (FJH) reactor can be employed to induce up to 3,000 K between the two electrodes filled with a carbon source. The FJH reactor could be automated onto a continuous manufacturing product line, by integrating the electrodes with a piston or onto a belt to continuously feed coal powders and collect graphitized products.<sup>5</sup>

## CONCLUSION AND OUTLOOK

This perspective highlights the role that complexity and tunability of HCMs (coal, tar, pitch, etc.) play in their thermal upgrading processes for a range of potential applications, from tar-based transparent heaters to supercapacitors to strain sensors. In addition to processing temperatures and ramping/cooling rates, the native chemistries of HCMs play a crucial role in the carbon product crystallinities, morphologies, and conductivities, among other properties. By controlling the initial H:C ratios and  $sp^2$  content of HCMs, products distributed from semiconductive hydrocarbon (optical bandgap 0–1.8 eV) to highly conductive ( $10^1$ ~ $10^3$  S/cm) carbon can be achieved by annealing.

Laser annealing and molecular dynamics simulations can be used to provide general guidelines to select the candidate of HCMs for target properties, and in the future, we expect ML methods to be a valuable direction together with continuous manufacturing for high-throughput HCMs screening, toward a consistent and flexible manufacturing process.

## ACKNOWLEDGMENTS

X.Z. acknowledges the support by start-up funding of Tsinghua University, Tsinghua University Initiative Scientific Research Program. C.J. acknowledges helpful discussions with Hasan Imani Parashkooh.

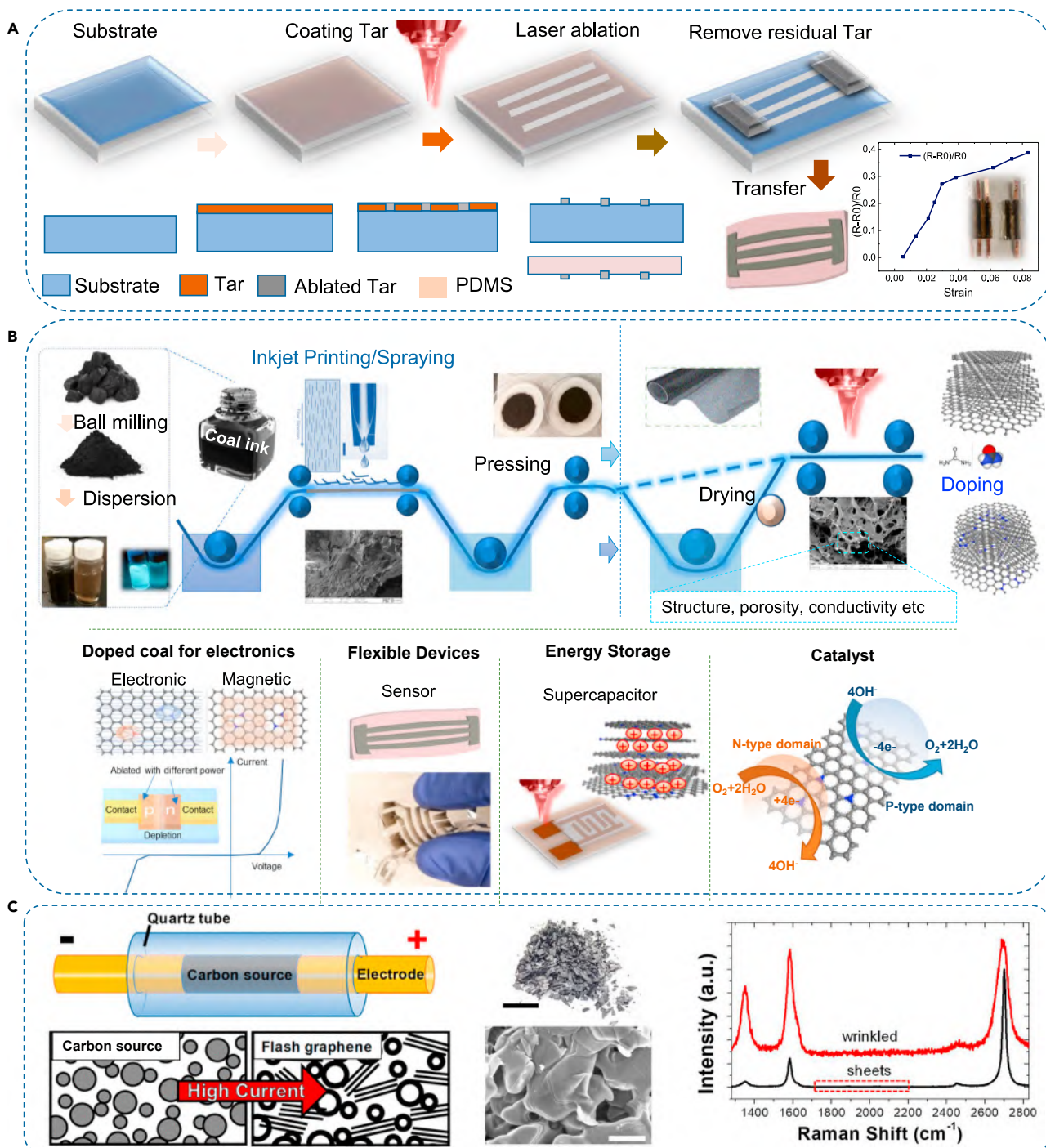


**Figure 6. A comparison and outlook of different manufacturing methods for large-scale applications of HCMs**

(A) Transformative manufacturing method to make tar-based thin-film flexible and stretchable devices.<sup>14</sup> Copyright ©2020, AAAS.

(B) A strategy of roll-to-roll manufacturing of coal-based thin film for a variety of applications.

(C) An FJH set up that can synthesis graphene at gram scale, which can be automated for continuous flash graphene (FG) synthesis using coal powder as carbon feedstock.<sup>5</sup> Copyright © 2020, American Chemical Society.<sup>120</sup>

## DECLARATION OF INTERESTS

The authors declare no competing interests.

## REFERENCES

1. Hasselmann, K. (1997). Climate-change research after Kyoto. *Nature* 390, 225–226.
2. Chu, S., and Majumdar, A. (2012). Opportunities and challenges for a sustainable energy future. *Nature* 488, 294–303.
3. Powell, C.A., and Moreale, B.D. (2008). Materials challenges in advanced coal conversion technologies. *MRS Bull* 33, 309–315.
4. Ali, S., Atkins, R., Bajura, R., Collins, D., Denton, D., Duddy, J., et al. (2019). Coal in a new carbon age powering a wave of innovation in advanced products & manufacturing (National Coal Council).
5. Luong, D.X., Bets, K.V., Algozeeb, W.A., Stanford, M.G., Kittrell, C., Chen, W., Salvatierra, R.V., Ren, M., McHugh, E.A., Advincula, P.A., et al. (2020). Gram-scale bottom-up flash graphene synthesis. *Nature* 577, 647–651.
6. Zhang, B., Rane, K., and Goual, L. (2020). Coal-derived nanomaterials for enhanced NAPL flow in porous media. *Carbon* 170, 439–451.
7. González, D., Montes-Morán, M.A., and García, A.B. (2003). Graphite materials prepared from an anthracite: a structural characterization. *Energy and Fuels* 17, 1324–1329.
8. Coal Market. (2020). <https://www.eia.gov/coal/>.
9. Abdulsalam, J., Mulopo, J., Oboirien, B., Bada, S., and Falcon, R. (2019). Experimental evaluation of activated carbon derived from South Africa discard coal for natural gas storage. *Int. J. Coal Sci. Technol.* 6, 459–477.
10. Jiang, X., Zhang, L., Wang, F., Liu, Y., Guo, Q., and Wang, C. (2016). Investigation of carbon black production from coal tar via chemical looping pyrolysis. *Energy Fuels* 30, 3535–3540.
11. Liu, J., Chen, X., Liang, D., and Xie, Q. (2020). Development of pitch-based carbon fibers: a review. *Energy Sourc. A Recover. Util. Environ. Eff.* 1–21.
12. Otani, S. (1981). Carbonaceous mesophase and carbon fibers. *Mol. Cryst. Liq. Cryst.* 63, 249–263.
13. Keller, B.D., Ferralis, N., and Grossman, J.C. (2016). Rethinking coal: thin films of solution processed natural carbon nanoparticles for electronic devices. *Nano Lett.* 16, 2951–2957.
14. Zang, X., Jian, C., Ingersoll, S., Li, H., Adams, J.J., Lu, Z., Ferralis, N., and Grossman, J.C. (2020). Laser-engineered heavy hydrocarbons: old materials with new opportunities. *Sci. Adv.* 6, 1–10.
15. Nielewski, L., Mendoza, K., Jalilov, A.S., Berka, V., Wu, G., Sikkema, W.K.A., Metzger, A., Ye, R., Zhang, R., Luong, D.X., et al. (2019). Highly oxidized graphene quantum dots from coal as efficient antioxidants. *ACS Appl. Mater. Inter.* 11, 16815–16821.
16. Ye, R., Peng, Z., Metzger, A., Lin, J., Mann, J.A., Huang, K., Xiang, C., Fan, X., Samuel, E.L.G., Alemany, L.B., et al. (2015). Bandgap engineering of coal-derived graphene quantum dots. *ACS Appl. Mater. Interfaces* 7, 7041–7048.
17. Parr, S.W. (1922). The classification of coal. *J. Ind. Eng. Chem.* 14, 919–922.
18. ASTM (2002). Standard Classification of Coals by Rank, 05.06 (Annu. B. ASTM Standards).
19. Zhao, Y., Liu, S., Elsworth, D., Jiang, Y., and Zhu, J. (2014). Pore structure characterization of coal by synchrotron small-angle X-ray scattering and transmission electron microscopy. *Energy Fuels* 28, 3704–3711.
20. Jean, J., Brown, P.R., Jaffe, R.L., Buonassisi, T., and Bulović, V. (2015). Pathways for solar photovoltaics. *Energy Environ. Sci.* 8, 1200–1219.
21. Zhang, C., Xie, Y., Zhang, C., and Lin, J. (2019). Upgrading coal to multifunctional graphene based materials by direct laser scribing. *Carbon* 153, 585–591.
22. Ye, R., Xiang, C., Lin, J., Peng, Z., Huang, K., Yan, Z., Cook, N.P., Samuel, E.L.G., Hwang, C.-C., Ruan, G., et al. (2013). Coal as an abundant source of graphene quantum dots. *Nat. Commun.* 4, 2943.
23. Sasikala, S.P., Henry, L., Yesilbag Tonga, G., Huang, K., Das, R., Giroire, B., Marre, S., Rotello, V.M., Penicaud, A., Poulin, P., and Aymonier, C. (2016). High yield synthesis of aspect ratio controlled graphenic materials from anthracite coal in supercritical fluids. *ACS Nano* 10, 5293–5303.
24. Powell, C., and Beall, G.W. (2015). Graphene oxide and graphene from low grade coal: synthesis, characterization and applications. *Curr. Opin. Colloid Interf. Sci.* 20, 362–366.
25. Leandro, A.P.M., Seas, M.A., Vap, K., Tyrrell, A.S., Jain, V., Wahab, H., and Johnson, P.A. (2021). Evolution of structural and electrical properties in coal-derived graphene oxide nanomaterials during high-temperature annealing. *Diam. Relat. Mater.* 112, 108244.
26. Xiao, F., Yang, S.X., Zhang, Z.Y., Liu, H.F., Xiao, J.W., Wan, L., Luo, J., Wang, S., and Liu, Y.Q. (2015). Scalable synthesis of freestanding sandwich-structured graphene/polyaniline/graphene nanocomposite paper for flexible all-solid-state supercapacitor. *Sci. Rep.* 5, 1–8.
27. Wang, Z., Zhao, Z., and Qiu, J. (2006). Synthesis of branched carbon nanotubes from coal. *Carbon* 44, 1321–1324.
28. Moothi, K., Iyuke, S.E., Meyyappan, M., and Falcon, R. (2012). Coal as a carbon source for carbon nanotube synthesis. *Carbon* 50, 2679–2690.
29. Speight, J.G. (2012). *The Chemistry and Technology of Coal*, Third Edition (CRC Press).
30. Bernardi, M., Lohrman, J., Kumar, P.V., Kirkeminde, A., Ferralis, N., Grossman, J.C., and Ren, S. (2012). Nanocarbon-based photovoltaics. *ACS Nano* 6, 8896–8903.
31. Li, H., Zhu, T., Ferralis, N., and Grossman, J.C. (2019). Charge transport in highly heterogeneous natural carbonaceous materials. *Adv. Funct. Mater.* 29, 1904283.
32. Awasthi, S., Awasthi, K., Ghosh, A.K., Srivastava, S.K., and Srivastava, O.N. (2015). Formation of single and multi-walled carbon nanotubes and graphene from Indian bituminous coal. *Fuel* 147, 35–42.
33. Du, A.B., Liu, X.G., Fu, D.J., Han, P.D., and Xu, B.S. (2007). Onion-like fullerenes synthesis from coal. *Fuel* 86, 294–298.
34. Zhou, Q., Zhao, Z., Zhang, Y., Meng, B., Zhou, A., and Qiu, J. (2012). Graphene sheets from graphitized anthracite coal: preparation, decoration, and application. *Energy and Fuels* 26, 5186–5192.
35. Kumar Thiyagarajan, S., Raghupathy, S., Palanivel, D., Raji, K., and Ramamurthy, P. (2016). Fluorescent carbon nano dots from lignite: unveiling the impeccable evidence for quantum confinement. *Phys. Chem. Chem. Phys.* 18, 12065–12073.
36. Apsley, N., and Hughes, H.P. (1975). Temperature- and field-dependence of hopping conduction in disordered systems, II. *Philos. Mag.* 31, 1327–1339.
37. Hao, Y., Tian, M., Zhao, H., Qu, L., Zhu, S., Zhang, X., Chen, S., Wang, K., and Ran, J. (2018). High efficiency electrothermal graphene/tourmaline composite fabric joule heater with durable abrasion resistance via a spray coating route. *Ind. Eng. Chem. Res.* 57, 13437–13448.
38. Raji, A.R.O., Varadachary, T., Nan, K., Wang, T., Lin, J., Ji, Y., Genorio, B., Zhu, Y., Kittrell, C., and Tour, J.M. (2016). Composites of graphene nanoribbon stacks and epoxy for joule heating and deicing of surfaces. *ACS Appl. Mater. Inter.* 8, 3551–3556.
39. Morris, O.P., Zang, X., Gregg, A., Keller, B., Getachew, B., Ingessoll, S., Elsen, H.A., Disko, M.M., Ferralis, N., and Grossman, J.C. (2019). Natural carbon by-products for transparent heaters: the case of steam-cracker tar. *Adv. Mater.* 31, 1900331.
40. Mahadeva, S.K., Walus, K., and Stoeber, B. (2015). Paper as a platform for sensing applications and other devices: a review. *ACS Appl. Mater. Inter.* 7, 8345–8362.
41. Ostfeld, A.E., Deckman, I., Gaikwad, A.M., Lochner, C.M., and Arias, A.C. (2015). Screen printed passive components for flexible power electronics. *Sci. Rep.* 5, 1–11.

42. Yang, H.Y.D. (2005). Electromagnetics. *Electr. Eng. Handb.* 477–478.
43. Baeg, K., and Lee, J. (2020). Flexible electronic systems on plastic substrates and textiles for smart wearable technologies. *Adv. Mater. Technol.* 2000071, 1–19.
44. Ye, R., James, D.K., and Tour, J.M. (2018). Laser-induced graphene. *Acc. Chem. Res.* 51 (7), 1609–1620.
45. Tan, K.W., and Wiesner, U. (2019). Block copolymer self-assembly directed hierarchically structured materials from nonequilibrium transient laser heating. *Macromolecules* 52, 395–409.
46. Zang, X., Shen, C., Chu, Y., Li, B., Wei, M., Zhong, J., Sanghadasa, M., and Lin, L. (2018). Laser-induced molybdenum carbide-graphene composites for 3D foldable paper electronics. *Adv. Mater.* 30, 1800062.
47. Hu, H., Li, Q., Li, L., Teng, X., Feng, Z., Zhang, Y., and Wu, M. (2020). Review laser irradiation of electrode materials for energy storage and conversion. *Matter* 3, 95–126.
48. Lin, J., Peng, Z.W., Liu, Y.Y., Ruiz-Zepeda, F., Ye, R.Q., Samuel, E.L.G., Yacaman, M.J., Yakobson, B.I., and Tour, J.M. (2014). Laser-induced porous graphene films from commercial polymers. *Nat. Commun.* 5, 1–8.
49. Zang, X., Tai, K.Y., Jian, C., Shou, W., Matusik, W., Ferralis, N., and Grossman, J.C. (2020). Laser-induced tar-mediated sintering of metals and refractory carbides in air. *ACS Nano* 14, 10413–10420.
50. Xu, R., Hung, A., Zverev, A., Shen, C., Irie, L., Ding, G., Whitmeyer, M., Ren, L., Griffin, B., Melcher, J., et al. (2018). A Kirigami-Inspired, extremely stretchable, high areal-coverage micro-supercapacitor patch. In Proceedings of the IEEE International Conference on Micro Electro Mechanical Systems (MEMS), 2018Proceedings of the IEEE International Conference on Micro Electro Mechanical Systems (MEMS).
51. Chyan, Y., Ye, R., Li, Y., Singh, S.P., Arnusch, C.J., and Tour, J.M. (2018). Laser-induced graphene by multiple lasing: toward electronics on cloth, paper, and food. *ACS Nano* 12, 2176–2183.
52. Tan, K.W., Jung, B., Werner, J.G., Rhoades, E.R., Thompson, M.O., and Wiesner, U. (2015). Transient laser heating induced hierarchical porous structures from block copolymer-directed self-assembly. *Science* 349, 54–58.
53. Ferralis, N., Liu, Y., Bake, K.D., Pomerantz, A.E., and Grossman, J.C. (2015). Direct correlation between aromatization of carbon-rich organic matter and its visible electronic absorption edge. *Carbon* 88, 139–147.
54. Papanastasiou, D.T., Schultheiss, A., Muñoz-Rojas, D., Celle, C., Carella, A., Simonato, J.P., and Bellet, D. (2020). Transparent heaters: a review. *Adv. Funct. Mater.* 30, 1–33.
55. Ferrari, A.C., and Robertson, J. (2000). Interpretation of Raman spectra of disordered and amorphous carbon. *Phys. Rev. B* 61, 14095–14107.
56. Ferrari, A.C. (2007). Raman spectroscopy of graphene and graphite: disorder, electron-phonon coupling, doping and nonadiabatic effects. *Solid State Commun.* 143, 47–57.
57. Ferralis, N. (2010). Probing mechanical properties of graphene with Raman spectroscopy. *J. Mater. Sci.* 45, 5135–5149.
58. Matthews, M.J., Pimenta, M.A., Dresselhaus, G., Dresselhaus, M.S., and Endo, M. (1999). Origin of dispersive effects of the Raman D band in carbon materials. *Phys. Rev. B Condens. Matter Mater. Phys.* 59, R6585.
59. Pimenta, M.A., Dresselhaus, G., Dresselhaus, M.S., Cançado, L.G., Jorio, A., and Saito, R. (2007). Studying disorder in graphite-based systems by Raman spectroscopy. *Phys. Chem. Chem. Phys.* 9, 1276–1291.
60. Barros, E.B., Demir, N.S., Souza Filho, A.G., Mendes Filho, J., Jorio, A., Dresselhaus, G., and Dresselhaus, M.S. (2005). Raman spectroscopy of graphitic foams. *Phys. Rev. B Condens. Matter Mater. Phys.* 71, 1–5.
61. Wang, Y., and Weng, G.J. (2018). In *Electrical Conductivity of Carbon Nanotube- and Graphene-Based Nanocomposites BT - Micromechanics and Nanomechanics of Composite Solids*, S.A. Meguid and G.J. Weng, eds. (Springer International Publishing), pp. 123–156.
62. Murata, H., Nakajima, Y., Saitoh, N., Yoshizawa, N., Suemasu, T., and Toko, K. (2019). High-electrical-conductivity multilayer graphene formed by layer exchange with controlled thickness and interlayer. *Sci. Rep.* 9, 1–5.
63. Pantea, D., Darmstadt, H., Kaliaguine, S., and Roy, C. (2003). Electrical conductivity of conductive carbon blacks: influence of surface chemistry and topology. *Appl. Surf. Sci.* 217, 181–193.
64. Hauser, J.J. (1975). Hopping conductivity in amorphous carbon films. *Solid State Commun.* 17, 1577–1580.
65. Liu, D., Lou, B., Chang, G., Zhang, Y., Yu, R., Li, Z., Wu, C., Li, M., and Chen, Q. (2018). Study on effect of cross-linked structures induced by oxidative treatment of aromatic hydrocarbon oil on subsequent carbonized behaviors. *Fuel* 231, 495–506.
66. Jiang, Y., Wang, P., Zang, X., Yang, Y., Kozinda, A., and Lin, L. (2013). Uniformly embedded metal oxide nanoparticles in vertically aligned carbon nanotube forests as pseudocapacitor electrodes for enhanced energy storage. *Nano Lett.* 13, 3524–3530.
67. Zhou, C., and Birney, D.M. (2002). A density functional theory study clarifying the reactions of conjugated ketenes with formaldimine. A plethora of pericyclic and pseudopericyclic pathways. *J. Am. Chem. Soc.* 124, 5231–5241.
68. Roberts, M.J., Everson, R.C., Domazetis, G., Neomagus, H.W.J.P., Jones, J.M., Van Sittert, C.G.C.E., Okolo, G.N., Van Niekerk, D., and Mathews, J.P. (2015). Density functional theory molecular modelling and experimental particle kinetics for CO<sub>2</sub>-char gasification. *Carbon* 93, 295–314.
69. Van Steenberge, P.H.M., Vandenbergh, J., D'Hooge, D.R., Reyniers, M.F., Adriaensens, P.J., Lutzen, L., Vanderzande, D.J.M., and Marin, G.B. (2011). Kinetic Monte Carlo modeling of the sulfinyl precursor route for poly(p-phenylene vinylene) synthesis. *Macromolecules* 44, 8716–8726.
70. van Duin, A.C.T., Dasgupta, S., Lorant, F., and Goddard, W.A., III (2001). ReaxFF: a reactive force field for hydrocarbons. *J. Phys. Chem. A* 105, 9396–9409.
71. Castro-Marcano, F., Kamat, A.M., Russo, M.F., van Duin, A.C.T., and Mathews, J.P. (2012). Combustion of an Illinois No. 6 coal char simulated using an atomistic char representation and the ReaxFF reactive force field. *Combust. Flame* 159, 1272–1285.
72. Mathews, J.P., and Chaffee, A.L. (2012). The molecular representations of coal - a review. *Fuel* 96, 1–14.
73. Wang, C., Watson, J.K., Louw, E., and Mathews, J.P. (2015). Construction strategy for atomistic models of coal chars capturing stacking diversity and pore size distribution. *Energy Fuels* 29, 4814–4826.
74. Fernandez-Alos, V., Watson, J.K., van der Wal, R., and Mathews, J.P. (2011). Soot and char molecular representations generated directly from HRTEM lattice fringe images using Fringe3D. *Combust. Flame* 158, 1807–1813.
75. Xin, H., Wang, C., Louw, E., Wang, D., and Mathews, J.P. (2016). Atomistic simulation of coal char isothermal oxy-fuel combustion: char reactivity and behavior. *Fuel* 182, 935–943.
76. Jian, C., Adams, J.J., Grossman, J.C., and Ferralis, N. (2021). Carbon fiber synthesis from pitch: insights from ReaxFF based molecular dynamics simulations. *Carbon* 176, 569–579.
77. Jian, C., Merchant, S., Zang, X., Ferralis, N., and Grossman, J.C. (2019). Structural evolutions of small aromatic mixtures under extreme temperature conditions: insights from reaxff molecular dynamics investigations. *Carbon* 155, 309–319.
78. Korai, Y., Yoon, S.-H., Oka, H., Mochida, I., Nakamura, T., Kato, I., and Sakai, Y. (1998). The properties of Co-oligomerized mesophase pitch from methylnaphthalene and naphthalene catalyzed by HF/BF<sub>3</sub>. *Carbon* 36, 369–375.
79. Jian, C., Poopari, M.R., Liu, Q., Zerpa, N., Zeng, H., and Tang, T. (2016). Reduction of water/oil interfacial tension by model asphaltenes: the governing role of surface concentration. *J. Phys. Chem. B* 120, 5646–5654.
80. Meneksedag-Erol, D., Tang, T., and Uludağ, H. (2014). Molecular modeling of polynucleotide complexes. *Biomaterials* 35, 7068–7076.
81. Du, J., and Rimsza, J.M. (2017). Atomistic computer simulations of water interactions and dissolution of inorganic glasses. *Npj Mater. Degrad.* 1, 16.
82. Duy, L.X., Peng, Z., Li, Y., Zhang, J., Ji, Y., and Tour, J.M. (2018). Laser-induced graphene fibers. *Carbon* 126, 472–479.
83. Zhang, Z., Song, M., Hao, J., Wu, K., Li, C., and Hu, C. (2018). Visible light laser-induced graphene from phenolic resin: a new approach for directly writing graphene-based

- electrochemical devices on various substrates. *Carbon* 127, 287–296.
84. Beckham, J.L., Li, J.T., Stanford, M.G., Chen, W., McHugh, E.A., Advincula, P.A., Wyss, K.M., Chyan, Y., Boldman, W.L., Rack, P.D., and Tour, J.M. (2021). High-resolution laser-induced graphene from photoresist. *ACS Nano* 15, 8976–8983.
  85. Wang, Q.-D., Wang, J.-B., Li, J.-Q., Tan, N.-X., and Li, X.-Y. (2011). Reactive molecular dynamics simulation and chemical kinetic modeling of pyrolysis and combustion of N-dodecane. *Combust. Flame* 158, 217–226.
  86. Li, G.-Y., Wang, F., Wang, J.-P., Li, Y.-Y., Li, A.-Q., and Liang, Y.-H. (2016). ReaxFF and DFT study on the sulfur transformation mechanism during the oxidation process of lignite. *Fuel* 181, 238–247.
  87. Shaw, D.E., Dror, R.O., Salmon, J.K., Grossman, J.P., MacKenzie, K.M., Bank, J.A., Young, C., Deneroff, M.M., Batson, B., Bowers, K.J., et al. (2009). Millisecond-scale molecular dynamics simulations on Anton. In Proceedings of the International Conference for High Performance Computing, Networking, Storage and Analysis SC'09, pp. 1–11.
  88. Dror, R.O., Jensen, M., Borhani, D.W., and Shaw, D.E. (2010). Perspectives on: molecular dynamics and computational methods exploring atomic resolution physiology on a femtosecond to millisecond timescale using molecular dynamics simulations. *J. Gen. Physiol.* 135, 555–562.
  89. Xie, T., France-Lanord, A., Wang, Y., Shao-Horn, Y., and Grossman, J.C. (2019). Graph dynamical networks for unsupervised learning of atomic scale dynamics in materials. *Nat. Commun.* 10, 1–9.
  90. Li, G.-Y., Ding, J.-X., Zhang, H., Hou, C.-X., Wang, F., Li, Y.-Y., and Liang, Y.-H. (2015). ReaxFF simulations of hydrothermal treatment of lignite and its impact on chemical structures. *Fuel* 154, 243–251.
  91. Bhoi, S., Banerjee, T., and Mohanty, K. (2014). Molecular dynamic simulation of spontaneous combustion and pyrolysis of brown coal using ReaxFF. *Fuel* 136, 326–333.
  92. Yuan, H., Kong, W., Liu, F., and Chen, D. (2019). Study on soot nucleation and growth from PAHs and some reactive species at flame temperatures by ReaxFF molecular dynamics. *Chem. Eng. Sci.* 195, 748–757.
  93. Jamrozik, A. (2017). The effect of the alcohol content in the fuel mixture on the performance and emissions of a direct injection diesel engine fueled with diesel-methanol and diesel-ethanol blends. *Energy Convers. Manag.* 148, 461–476.
  94. Kwon, H., Lele, A., Zhu, J., McEnally, C.S., Pfefferle, L.D., Xuan, Y., and van Duin, A.C.T. (2020). ReaxFF-based molecular dynamics study of bio-derived polycyclic alkanes as potential alternative jet fuels. *Fuel* 279, 118548.
  95. Igram, D., Bhattacharai, B., Biswas, P., and Drabold, D.A. (2018). Large and realistic models of amorphous silicon. *J. Non-Cryst. Sol.* 492, 27–32.
  96. Deringer, V.L., Bernstein, N., Bartók, A.P., Cliffe, M.J., Kerber, R.N., Marbella, L.E., Grey, C.P., Elliott, S.R., and Csányi, G. (2018). Realistic atomistic structure of amorphous silicon from machine-learning-driven molecular dynamics. *J. Phys. Chem. Lett.* 9, 2879–2885.
  97. Zhang, L., Hou, Z., Horton, S.R., Klein, M.T., Shi, Q., Zhao, S., and Xu, C. (2014). Molecular representation of petroleum vacuum resid. *Energy Fuels* 28, 1736–1749.
  98. Agarwal, P., Sahasrabudhe, M., Khandalkar, S., Saravanan, C., and Klein, M.T. (2019). Molecular-level kinetic modeling of a real vacuum gas oil hydropyrolysis refinery system. *Energy Fuels* 33, 10143–10158.
  99. Deringer, V.L., and Csányi, G. (2017). Machine learning based interatomic potential for amorphous carbon. *Phys. Rev. B* 95, 1–15.
  100. Jana, R., Savio, D., Deringer, V.L., and Pastewka, L. (2019). Structural and elastic properties of amorphous carbon from simulated quenching at low rates. *Model. Simul. Mater. Sci. Eng.* 27, 085009.
  101. Rajan, K., Suh, C., and Mendez, P.F. (2009). Principal component analysis and dimensional analysis as materials informatics tools to reduce dimensionality in materials science and engineering. *Stat. Anal. Data Min. ASA Data Sci. J.* 1, 361–371.
  102. Zang, X., Jian, C., Zhu, T., Fan, Z., Wang, W., Wei, M., Li, B., Follmar Diaz, M., Ashby, P., Lu, Z., et al. (2019). Laser-sculptured ultrathin transition metal carbide layers for energy storage and energy harvesting applications. *Nat. Commun.* 10, 3112.
  103. Zhang, L., Han, J., Wang, H., Car, R., and E, W. (2018). Deep potential molecular dynamics: a scalable model with the accuracy of quantum mechanics. *Phys. Rev. Lett.* 120, 143001.
  104. Lu, D., Wang, H., Chen, M., Lin, L., Car, R., E, W., Jia, W., and Zhang, L. (2021). 86 PFLOPS deep potential molecular dynamics simulation of 100 million atoms with ab initio accuracy. *Comput. Phys. Commun.* 259, 107624.
  105. Wei, W., Bennett, C.A., Tanaka, R., Hou, G., Klein, M.T., and Klein, M.T. (2008). Computer aided kinetic modeling with KMT and KME. *Fuel Process. Technol.* 89, 350–363.
  106. Jin, Z., Zhang, Z., Demir, K., and Gu, G.X. (2020). Machine learning for advanced additive manufacturing. *Matter* 3, 1541–1556.
  107. Hsu, Y.C., Yu, C.H., and Buehler, M.J. (2020). Using deep learning to predict fracture patterns in crystalline solids. *Matter* 3, 197–211.
  108. Dijkstra, M., and Luijten, E. (2021). From predictive modelling to machine learning and reverse engineering of colloidal self-assembly. *Nat. Mater.* 20, 762–773.
  109. Friederich, P., Häse, F., Proppe, J., and Aspuru-Guzik, A. (2021). Machine-learned potentials for next-generation matter simulations. *Nat. Mater.* 20, 750–761.
  110. Louie, S.G., Chan, Y., da Jornada, F.H., Li, Z., and Qiu, D.Y. (2021). Discovering and understanding materials through computation. *Nat. Mater.* 20, 728–735.
  111. Liu, Y., Ferralis, N., Bryndzia, L.T., and Grossman, J.C. (2016). Genome-inspired molecular identification in organic matter via Raman spectroscopy. *Carbon N. Y.* 101, 361–367.
  112. Salley, D., Keenan, G., Grizou, J., Sharma, A., Martín, S., and Cronin, L. (2020). A nanomaterials discovery robot for the Darwinian evolution of shape programmable gold nanoparticles. *Nat. Commun.* 11, 1–7.
  113. Wahab, H., Jain, V., Tyrrell, A.S., Seas, M.A., Kotthoff, L., and Johnson, P.A. (2020). Machine-learning-assisted fabrication: Bayesian optimization of laser-induced graphene patterning using in-situ Raman analysis. *Carbon* 167, 609–619.
  114. Sengul, M.Y., Song, Y., Nayir, N., Gao, Y., Hung, Y., Dasgupta, T., and van Duin, A.C.T. (2021). INDEEDopt: a deep learning-based ReaxFF parameterization framework. *Npj Comput. Mater.* 7, 1–9.
  115. Botu, V., and Ramprasad, R. (2015). Learning scheme to predict atomic forces and accelerate materials simulations. *Phys. Rev. B Condens. Matter Mater. Phys.* 92, 1–5.
  116. Guo, F., Wen, Y.S., Feng, S.Q., Li, X.D., Li, H.S., Cui, S.X., Zhang, Z.R., Hu, H.Q., Zhang, G.Q., and Cheng, X.L. (2020). Intelligent-ReaxFF: evaluating the reactive force field parameters with machine learning. *Comput. Phys. Mater. Sci.* 172, 109393.
  117. Schütt, K.T., Sauceda, H.E., Kindermans, P.J., Tkatchenko, A., and Müller, K.R. (2018). SchNet - a deep learning architecture for molecules and materials. *J. Chem. Phys.* 148, 241722.
  118. Cranford, S.W., Chin, S., and Sun, J. (2019). The “what” and “why” of materials. *Matter* 1, 1–3.
  119. Julia, W., Academies, N., and Materials, N. (2020). Julia Greer Answers Questions about additive manufacturing. *Nat. Commun.* 11, 3993.
  120. Yakobson, B.I., Tour, J.M., Stanford, M.G., Bets, K.V., Luong, D.X., Advincula, P.A., Chen, W., Li, J.T., Wang, Z., McHugh, E.A., and Algozeen, W.A. (2020). Flash graphene morphologies. *ACS Nano* 14, 13691–13699.
  121. Delacroix, S., Wang, H., Heil, T., and Strauss, V. (2020). Laser-induced carbonization of natural organic precursors for flexible electronics. *Adv. Electron. Mater.* 6, 1–8.